



Cite this: *Soft Matter*, 2021,
17, 1663

Gauge invariant and gauge dependent aspects of topological walking colloidal bipeds[†]

Mahla Mirzaee-Kakhki,^a Adrian Ernst,^a Daniel de las Heras,^a Maciej Urbaniak,^b Feliks Stobiecki,^b Andreea Tomita,^c Rico Huhnstock,^c Iris Koch,^c Arno Ehresmann,^c Dennis Holzinger^c and Thomas M. Fischer^a ^{*a}

Paramagnetic colloidal spheres assemble to colloidal bipeds of various length in an external magnetic field. When the bipeds reside above a magnetic pattern and we modulate the direction of the external magnetic field, the rods perform topologically distinct classes of protected motion above the pattern. The topological protection allows each class to be robust against small continuous deformations of the driving loop of the external field. We observe motion of the rod from a passive central sliding and rolling motion for short bipeds toward a walking motion with both ends of the rod alternately touching down on the pattern for long bipeds. The change of character of the motion occurs in form of discrete topological transitions. The topological protection makes walking a form of motion robust against the breaking of the non-symmorphic symmetry. In patterns with non-symmorphic symmetry walking is reversible. In symmorphic patterns lacking a glide plane the walking can be irreversible or reversible involving or not involving ratchet jumps. Using different gauges allows us to unravel the active and passive aspects of the topological walks.

Received 16th September 2020,
Accepted 10th December 2020

DOI: 10.1039/d0sm01670e

rsc.li/soft-matter-journal

1 Rolling, walking, and limping

Rolling is a process where a wheel winds around its axis and thereby translates on a support. If the propulsion distance of the wheel matches the wheel circumsphere the rolling is with a non-slip condition. Otherwise the rolling is with slip. Walking is generically a symmetric process differing from rolling. A walker progresses in steps by moving his feet and depending on the number of feet we call the walker a biped, tripod, quadruped etc. A human is an example of a biped, where both feet of a walking person perform alternating steps. The spatial period of the walk of a biped is two steps, – not one step –, since the conformation of a person is restored after two steps and the conformation after an odd number of steps is related to the conformation after an even number of steps by a non-symmorphic group operation (a half period translation followed by a reflection known as a glide plane). The non-symmorphic symmetry can be broken in a trivial manner for example by

breaking one of our legs in which case we start limping and the broken leg functions differently than its non-broken mirror image partner.

We may view symmetric walking as a symmetry reduced form of rolling and limping as a symmetry reduced form of walking. For a rolling wheel all orientations of the wheel are of equivalent importance. A full rotation of the wheel passes through all equivalent orientations of the wheel in a continuous way. For a symmetric walker the symmetry of the motion is reduced to a two-fold discrete symmetry as compared to the continuous symmetry of the wheel. The symmetry is further reduced when the walker limps.

A subtle, albeit psychologically undesirable¹ way of breaking the non-symmorphic symmetry of a symmetric walker is by letting him walk on a periodic structure with a period of the pattern commensurable with his step width. If the pattern has the period of one step but lacks the mirror symmetry of the non-symmorphic group operation of our two-step-periodic walker, we expect one foot to perform in a symmetry broken way compared to the other foot. One example of such walking is the motor protein Kinesin. It accomplishes transport by walking with its two heads (not its two feet) along a microtubule. The microtubule is a chiral periodic structure that lacks mirror symmetries such that we expect differences between the two heads even when the two heads walk in a “hand-over-hand” mechanism, where the kinesin heads step past one another, alternating the lead position.^{2,3}

^a University of Bayreuth, Physics, Universitätsstr. 30, 95447 Bayreuth, Germany.
E-mail: Thomas.Fischer@uni-bayreuth.de

^b Institute of Molecular Physics, Polish Academy of Sciences,
ul. M. Smoluchowskiego 17, 60-179 Poznań, Poland

^c Institute of Physics and Center for Interdisciplinary Nanostructure Science
and Technology (CINSat), University of Kassel, Heinrich-Plett-Strasse 40, D-34132
Kassel, Germany

[†] Electronic supplementary information (ESI) available. See DOI: 10.1039/d0sm01670e

A subtle way to allow for symmetric walking on a periodic pattern is to use a pattern with primitive unit vectors of two steps. If the space group of the pattern is non-symmorphic, containing the non-symmorphic group operation of our walker, the walker can still walk in a symmetric way.

If instead we use a symmorphic pattern containing only symmorphic group elements the walker is expected to walk in a symmetry-broken way. Its left foot has to step onto a position that is not related by a symmetry operation to the position the right foot steps upon.

A further way of breaking the symmetry of a walker exists for driven systems, where the walker responds to external commands. If those commands lack a non-symmorphic symmetry in time our walker will perform a walk lacking the non-symmorphic glide symmetry.

2 Robust walking

Rolling and walking are both usually generated by a cyclic change of certain parameters that control and drive the motion. These parameters can be as diverse as certain signals of the spinal chord for walking humans^{4,5} or walking animals,⁶ the concentration of complementary DNA-strands as well as temperature in DNA-bipeds,⁷ or the geometric shape for geometric swimmers at low Reynolds numbers.^{8,9} We can thus define a control space \mathcal{C} that is the space of possible parameters that might occur while we drive the motion. For robust walking the result of a slightly perturbed loop in control space \mathcal{C} must result in a successful sequence of walking steps albeit the disturbance of the loop. For robotic walkers mathematical algorithms such as Lyapunov function based control algorithms or control barrier functions are employed to guarantee safe walking.¹⁰ Another powerful way of ensuring such robust behavior is the use of topological invariants.^{11–23} If the control space \mathcal{C} is a not simply connected space the winding number $w(\mathcal{L}_c)$ of a loop \mathcal{L}_c around the holes in control space constitutes a topological invariant. A walk on a pattern is a topological walk if the number of steps $n_{\text{step}} = mw(\mathcal{L}_c)$ on the pattern is a non zero but low integer multiple ($m = \pm 1, \pm 2, \dots$) of the winding number irrespective of the details of how precisely and with which speed the loop in control space winds around a hole.

This robustness includes perturbations that break the non-symmorphic symmetry. When the walking is topologically robust, then the stronger foot of the walker must consistently make up for its weaker partner in order to secure the commensurability with the period of the pattern. The robustness, however, also holds when we extend the two fold symmetry of a walker to the continuous symmetry of a rolling wheel. The space of orientations of a wheel is a not simply connected space and thus topological invariants can be used to control their motion on a pattern. In this work we morph the topological sliding rolling of a colloidal wheel into the topological equivalent motion of self assembled colloidal rods that either slide and roll or walk on symmorphic and non-symmorphic magnetic lattices. We show the topological robustness of the

transport by successively deforming the wheel into a biped and by continuously changing the character of the motion from rolling toward walking. Topological transitions toward larger bipeds with discretely increasing step widths occur as the self assembled biped grows longer.

3 Experimental setup

We illustrate the richness of biped motion using a square magnetic lattice (Fig. 1a)^{24,25} with a glide plane and a magnetic hexagonal lattice (Fig. 1c) containing no glide plane. We study experimentally and with computer simulations the character of the biped motion. In the experiments, paramagnetic colloidal particles (negatively charged COOH-functionalized paramagnetic Dynabeads M-270 of radius $R = 1.4 \mu\text{m}$ and effective magnetic susceptibility $\chi_{\text{eff}} = 0.6$) assembled to a rod of $n = 2–11$ particles move above a thin Co/Au layered system with perpendicular magnetic anisotropy lithographically patterned *via* ion bombardment.^{25–27} The pattern consists of a square (hexagonal) lattice of magnetized domains with a mesoscopic pattern lattice constant $a \approx 7 \mu\text{m}$, see a sketch in Fig. 1a and c. The whole pattern is magnetized in the $\pm z$ -direction normal to the film. The magnetic pattern is spin coated with a $1.6 \mu\text{m}$ polymer film that serves as a spacer. The paramagnetic colloidal particles are immersed in water. A uniform time-dependent external magnetic field $\mathbf{H}_{\text{ext}}(t)$ of constant magnitude ($\mathbf{H}_{\text{ext}} = 4 \text{ kA m}^{-1}$) is superimposed to the non-uniform and time-independent magnetic field generated by the pattern \mathbf{H}_p . The external field $\mathbf{H}_{\text{ext}}(t)$ is varied on the surface of a sphere and hence the topology of our control space \mathcal{C} is that of a punctured sphere (certain bifurcation or fence points are removed from the sphere which renders the sphere not simply connected, see Fig. 1b and d). We perform periodic modulation loops \mathcal{L}_c of the external field in control space \mathcal{C} to drive the system. The external field is strong enough to cause the paramagnetic particles to assemble into a rod because of induced dipolar interactions between them. The two ends of the rod are the two feet of our self assembled biped. The dipolar interactions are stronger than the buoyancy of the biped causing the biped to align with the external field, which generically lifts one foot of the biped from the ground while the other foot remains on the ground. Note that the locking of the orientation of the biped to the external field with the continuous variation of the external field causes each foot to always keep its magnetic character, *i.e.* the northern foot located at \mathbf{r}_N being a magnetic north pole and the southern foot at \mathbf{r}_S being a south pole. The vector $\mathbf{b} = \mathbf{r}_S - \mathbf{r}_N$ denotes the northern foot to southern foot vector of the biped. The locking of the biped orientation \mathbf{b} to the external field \mathbf{H}_{ext} allows to interchangeably use the sphere of biped orientations or the sphere of external field orientations as the control space. The southern foot will be on the ground when the external field points into the south of \mathcal{C} . The northern foot will be on the ground when the external field points into the north of \mathcal{C} . The transfer of support between the two feet occurs when the external field is within the tropics of \mathcal{C} .

The external magnetic field has negligible lateral gradients and the position of the biped is governed by the field gradients

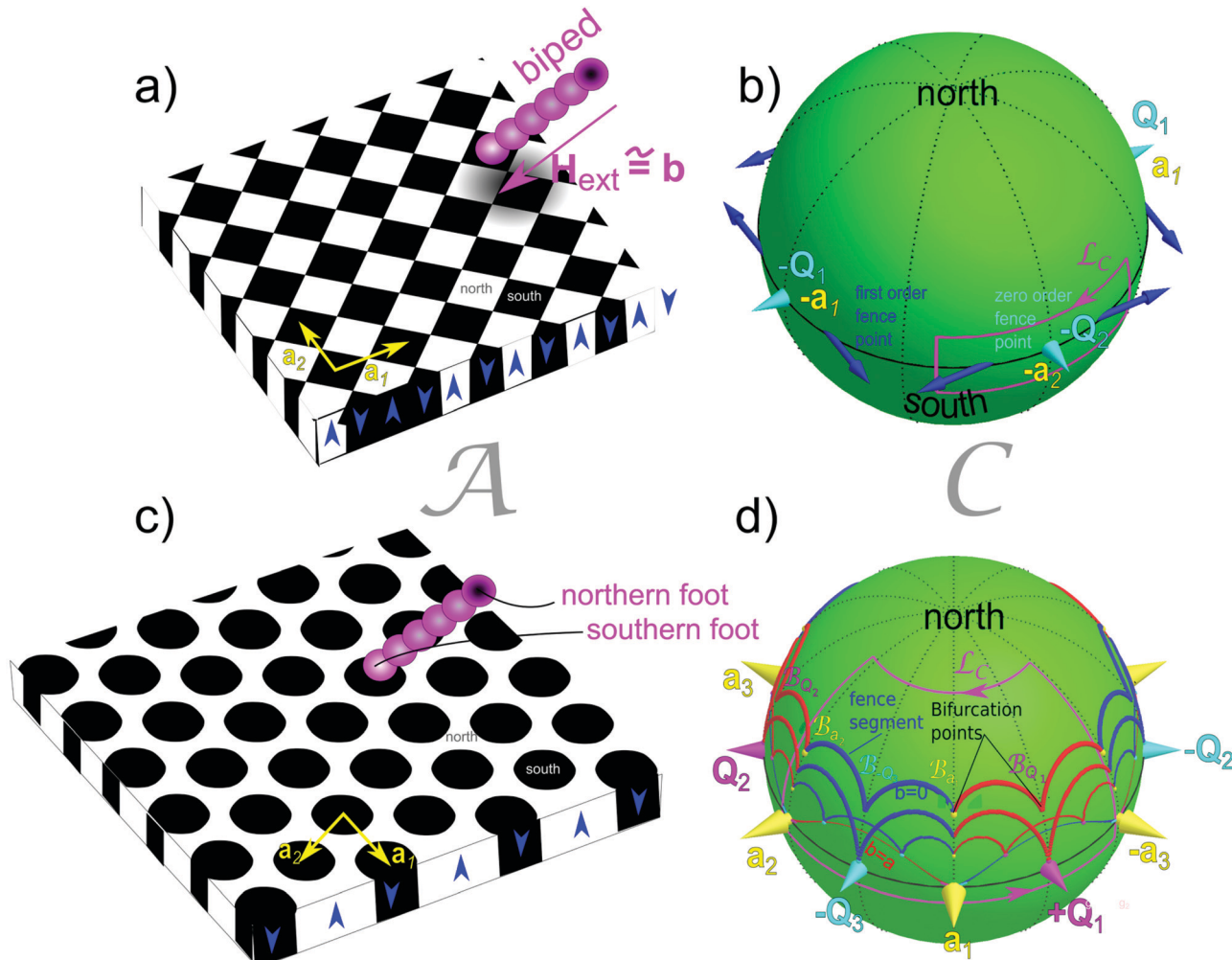


Fig. 1 (a) Square ((c) hexagonal) magnetic pattern with up (white) and down (black) magnetized regions, characterized by the primitive unit vectors \mathbf{a}_i (yellow) and primitive reciprocal unit vectors \mathbf{Q}_i (magenta). Colloids (magenta) assemble into a rod that functions as a biped with feet at both ends. The biped walks across the pattern as we apply modulation loops of the external magnetic field. The external field and thus the orientation \mathbf{b} varies on the surface of a sphere (b and d). The walk depends on how the modulation loops in control space wind around the fence points (segments) in control space (b and d) that in general vary with the length b of the biped. We show a typical fundamental loop \mathcal{L}_C (purple) that causes different topologically protected transport for small and larger bipeds. Fence points for the square lattice in (b) are the points pierced by the cyan and blue arrows. For the hexagonal lattice in (d) segments of fence lines are depicted in red and blue and they meet in bifurcation points where the curvature of the fence diverges.

of the magnetic pattern. These gradients decay exponentially with the distance from the pattern. Therefore, the location of the walker is with the grounded foot sitting within a local minimum of the colloidal potential (a foothold). The transfer of support is accompanied by a release of the lifting foot from the minimum of the colloidal potential and a sliding of the touching down foot into a new minimum (foothold). Generically, the transfer of support will be associated with frustration as the length $b = 2(n - 1)R$ of the biped will not match with the distance between consecutive minima.

4 Topological rolling transport of single spheres

Let us refer to the two-dimensional space the walker steps upon as action space \mathcal{A} . Special closed modulation loops in control

space \mathcal{C} induce open walks in action space \mathcal{A} . In ref. 24, 25 and 28 we demonstrated how the bulk rolling of single colloidal spheres (point particles) above magnetic lattices with different symmetries is topologically protected. We summarize here the main aspects of the sphere transport and refer the reader to ref. 24, 25 and 28 for a complete description. For each lattice symmetry there exist special fundamental modulation loops of \mathbf{H}_{ext} in \mathcal{C} that induce transport of colloids in \mathcal{A} by a primitive lattice vector \mathbf{a}_i . These fundamental loops share a common feature, they wind around special objects that lie in $\mathcal{C}^{24,25,28}$ roughly in the direction of a primitive reciprocal unit vector perpendicular to the primitive lattice vector \mathbf{a}_i of the transport. A sphere does not walk because it is isotropic and has no foot. It adiabatically slides or rolls²⁹ on an externally controlled time scale and for very particular non trivial loops on a square lattice and in half of the non trivial loops on hexagonal lattice it irreversibly slides on a faster intrinsic time scale. The character

of the transport thus is that of a wheel rolling with slip between the wheel and the ground.

In the simplest case, a square lattice, the control space is characterized by just four zero order “fence” points on the equator lying along the directions of the primitive reciprocal lattice vectors,²⁴ see Fig. 1b. For a hexagonal lattice the objects are fence segments connecting bifurcation points in \mathcal{C} , see Fig. 1d. We call a modulation loop encircling one of these objects a fundamental loop $\mathcal{L}_{\mathcal{Q}_i}$. Each of these fundamental loops induces adiabatic transport in the sense that a single colloidal particle follows a minimum of the colloidal potential at any time. Hence, the position of the particle in \mathcal{A} parametrically depends on the position of the external magnetic field in \mathcal{C} . All modulation loops discussed in what follows can be viewed as concatenations of fundamental loops. The motion of a sphere is an adiabatic motion if the loop is encircling the object without cutting through it.

5 Theory of adiabatic topological walks

Because the transport of a colloidal sphere is topological it is robust to perturbations. Mathematically the surface of a colloidal sphere is a manifold of genus $g = 0$ and it is topologically equivalent to a biped. In theory we may continuously distort the shape of a sphere into that of a biped. In experiments this distortion is achieved by an assembly of a discrete number of spheres into a biped rod rather than by continuously distorting a colloidal particle. If the perturbation introduced by this change of shape is not too strong the result of a control loop must be the same no matter whether the object is a sphere or a biped. Longer bipeds fall into topological equivalence classes that are different from that of a point particle.

We may write the pattern magnetic field as²⁴

$$\mathbf{H}_p = \nabla\psi \quad (1)$$

where

$$\psi(\mathbf{r}) \propto e^{-Qz} \sum_{n=1}^N \exp(i\mathbf{r}_A \cdot \mathbf{R}_N^n \cdot \mathbf{Q}_1) \quad (2)$$

is the magnetic potential and depends on the position $\mathbf{r} = (\mathbf{r}_A, z)$ that we have split into a lateral vector \mathbf{r}_A in action space \mathcal{A} and the normal component z . Making use of the periodicity of the pattern, topologically action space is equivalent to a torus. A path leading from one unit cell to a neighboring unit cell becomes a path that winds around the torus once. The vector \mathbf{Q}_1 denotes one of the N lowest non vanishing reciprocal lattice vectors of the 2D-lattice and $Q = 2\pi/a$ its modulus. The lattice is invariant under a 2D rotation \mathbf{R}_N by the angle $2\pi/N$ and the other $N - 1$ equivalent reciprocal lattice vectors are obtained by successive rotations $\mathbf{Q}_{n+1} = \mathbf{R}_N \mathbf{Q}_n$. The projection of the pattern magnetic field onto the external field and averaged over the biped is the biped potential

$$V_{\text{biped}} \propto \psi(\mathbf{r}_S) - \psi(\mathbf{r}_N) \quad (3)$$

where \mathbf{r}_S and \mathbf{r}_N are the positions of the southern and the northern foot of the biped. The vector $\mathbf{b} = \mathbf{r}_S - \mathbf{r}_N$ denotes the northern foot to southern foot vector of the biped. When the external magnetic field is strong compared to the pattern field the orientation \mathbf{b} is locked to the direction of the external field $\mathbf{b} \parallel \mathbf{H}_{\text{ext}}$. We may thus choose the vector space of \mathbf{b} as control space. In the limit $b \ll a$ the biped potential reduces to a point particle potential

$$V_{\text{point}} \propto \mathbf{b} \cdot \mathbf{H}_p \propto \mathbf{H}_{\text{ext}} \cdot \mathbf{H}_p \quad (4)$$

5.1 Gauges

We have discussed the topological properties of V_{point} in ref. 24, 25 and 28.

We would like to write the position of both feet as a sum of an absolute position and a conformational position

$$\mathbf{r}_{S/N} = \mathbf{r}_{\text{abs}} + \mathbf{r}_{\text{con}, S/N} \quad (5)$$

such that the conformation position after the period T of a closed fundamental control loop $\mathcal{L}_{\mathcal{C}}$ is restored

$$\mathbf{r}_{\text{conf}, S/N}(T) = \mathbf{r}_{\text{con}, S/N}(0) \quad (6)$$

and the translation $\Delta\mathbf{r}_{\text{abs}} = \mathbf{a}_i$ by lattice vector over a period is blamed onto the absolute position \mathbf{r}_{abs} . The decomposition eqn (5) carries a gauge freedom. We will make use of two choices of gauge. The center gauge simply chooses the absolute position to be the center of the biped $\mathbf{r} = \mathbf{r}_{\text{abs}} = (\mathbf{r}_S + \mathbf{r}_N)/2$ and the conformational coordinates as $\mathbf{r}_{\text{con}, S/N} = \pm\mathbf{b}/2$. This choice of gauge is useful since it splits the position into a vector $\mathbf{r} = (\mathbf{r}_A, z)$ in action space and a vector \mathbf{b} in control space. An alternative choice of the absolute position is the instantaneous center of rotation:

$$\mathbf{r}_{\text{Abs}} = \mathbf{r}_{\text{ICR}} \quad (7)$$

such that

$$d\mathbf{r}_{\text{ICR}} = d\mathbf{b} \cdot \nabla_{\mathbf{b}} \mathbf{r}_{\text{ICR}} = \mathbf{0} \quad (8)$$

exactly if

$$d\mathbf{b} \cdot \nabla_{\mathbf{b}} |\mathbf{r}_{\text{ICR}} - \mathbf{r}_S| = d\mathbf{b} \cdot \nabla_{\mathbf{b}} |\mathbf{r}_{\text{ICR}} - \mathbf{r}_N| = 0 \quad (9)$$

We call this gauge the walker gauge because eqn (9) will hold whenever the biped foot remains within a non moving foothold such that either $\mathbf{r}_{\text{ICR}} = \mathbf{r}_S$ or $\mathbf{r}_{\text{ICR}} = \mathbf{r}_N$. Eqn (8) and (9) state that the edge \mathbf{r}_{ICR} of the triangle defined by \mathbf{r}_S , \mathbf{r}_N and \mathbf{r}_{ICR} can only translate if the triangle changes its shape. In particular, the walker does not translate when one foot is grounded. The only translational motion of an ideal walker $d\mathbf{r}_{\text{ICR,ideal}} = \mathbf{b}_{\text{transfer}} \delta(t - t_{\text{transfer}})dt$ occurs when the instantaneous center of rotation longitudinally moves from one foot to the other by the momentary vector $\mathbf{b}_{\text{transfer}}$ during the transfer of support. The walker gauge shows how essential is the lift of one foot from the non moving foothold and the grounding of the next foot for effective walking. The center of an ideal walker in contrast moves on a circle around the grounded foot while one of the feet is grounded. It does not move when the grounding is transferred between the feet. The motion of the biped center and the instantaneous center of

rotation for a general ideal or non ideal walker are quite different. Nevertheless, the motion of both points over a period is the same and thus gauge independent because of eqn (6). We decompose the motion of the instantaneous center of rotation into a longitudinal and transversal component.

We anticipate the longitudinal component of the motion as the autonomous walking component of the motion. The transversal component arises if a foothold is moving. This motion is a passive transport of the walker with the foothold. The walker gauge is useful to decompose the motion into walking and passive advection. Note, however, that the decomposition into walking and advection in contrast to the full motion is gauge dependent.

6 Adiabatic walks on square patterns

6.1 Walkers gauge

In Fig. 2a we show the driving loop $\mathcal{L}_{Q_2}^{-1}(\Delta\phi)$ in the control space \mathcal{C} of a square pattern. The loop clockwise circulates the

fence point of $-Q_2$ direction with an azimuthal width of $\Delta\phi$. In Fig. 2b we plot simulated trajectories on square patterns of the southern (blue) and northern (red) foot together with the instantaneous center of rotation r_{ICR} that we color in green when the motion is longitudinal (along \mathbf{b}), orange when it is transversal, and white when it is a mixture of longitudinal and transversal motion. Two trajectories are shown. One for a small biped of length $b = 0.6a$ and one of a large biped of length $b = 2.8a$. The long biped longitudinally autonomously walks, while the smaller biped also shows some passive mixed sliding of the foothold (white part of the instantaneous center of rotation trajectory).

In Fig. 2c we plot experimental trajectories of the southern (blue) and the northern (red) foot of various bipeds assembled from colloidal spheres of radius $R = 2.8 \mu\text{m}$ on a square pattern of lattice constant $a = 7 \mu\text{m}$. We also plot the trajectory instantaneous center of rotation (green). All bipeds are subject to the loop $\mathcal{L}_{Q_2}^{-1}(\Delta\phi)$ of width $\Delta\phi = 65^\circ$. A video clip of bipeds

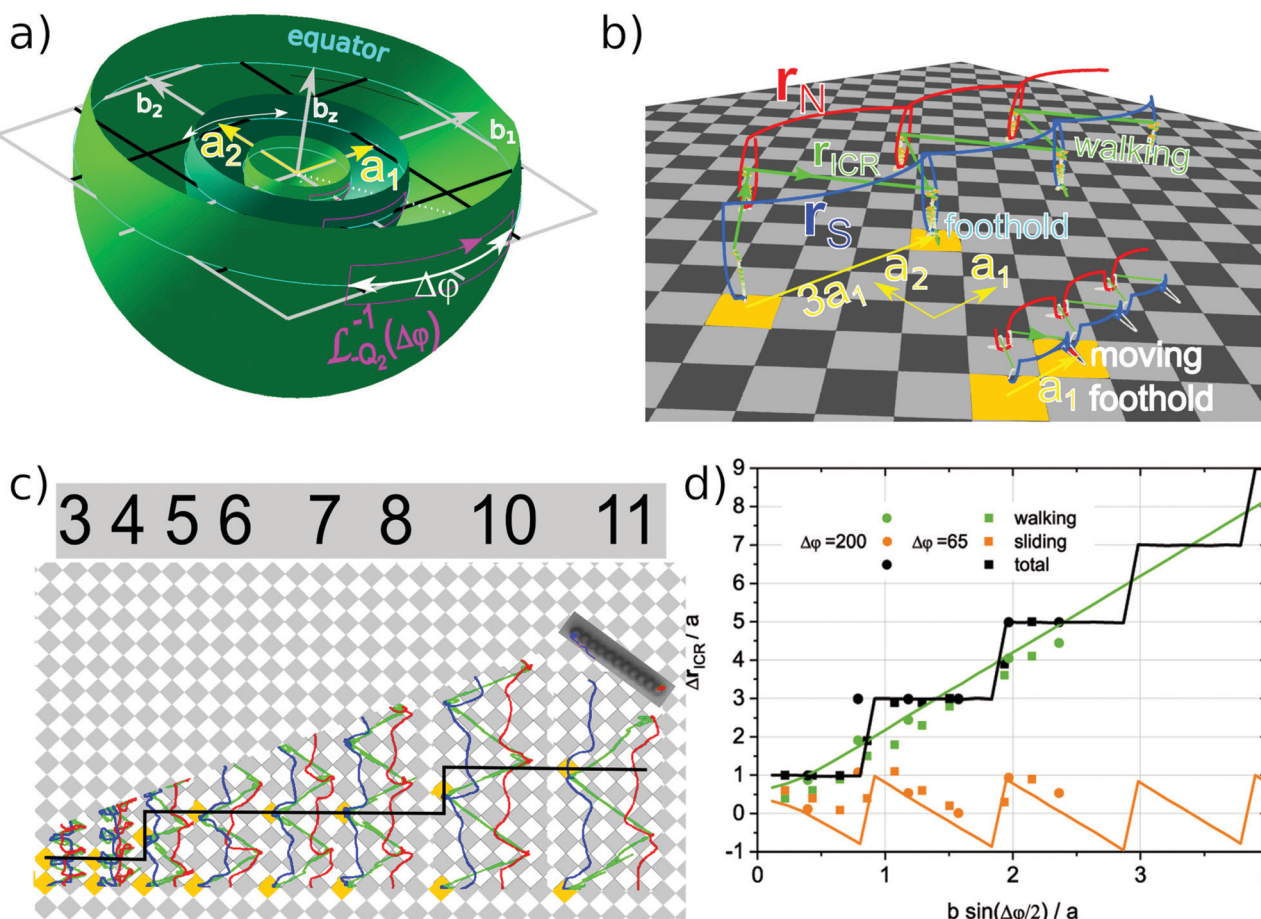


Fig. 2 (a) Control spaces of bipeds of lengths $b = 0.5a, 1.05a, 2.1a$ with a fundamental loop $\mathcal{L}_{Q_2}^{-1}(\Delta\phi)$ of width $\Delta\phi = 70^\circ$. Fence lines are drawn in gray and black. (b) Simulated trajectories of both feet (blue and red) and the instantaneous center of rotation r_{ICR} for a biped of length $b = 0.6a$ and $b = 2.8a$. Longitudinal moves of the instantaneous center of rotation are shown in green, transversal moves in orange and mixed moves in white. (c) Experimental trajectories of the feet (blue and red) of bipeds assembled from 3–11 colloidal spheres of radius $R = 2.8 \mu\text{m}$ on a square pattern of lattice constant $a = 7 \mu\text{m}$ are shown together with the path of the instantaneous center of rotation (green). We also overlay a microscope images of the final biped position of the 11-particle biped. Two consecutive footholds of the southern foot for each walker are marked in orange. (d) Plot of the simulated and experimentally determined total, longitudinal and transversal displacement of the instantaneous center of rotation subject to the loop of width $\Delta\phi = 70^\circ$ for the simulations and $\Delta\phi = 65^\circ$ and $\Delta\phi = 200^\circ$ for the experiments. Videoclips of bipeds subject to the same loop are shown in the Supplementary movie adfigure2.mp4.

of different lengths subject to this loop are shown in the video clip adfigure2.mp4. In Fig. 2c bipeds consisting of 3–11 colloidal particles are shown. Two consecutive footholds the southern foot steps upon are marked in orange to emphasize the step width of our walkers. We also overlay a microscope image of the final biped position for the 11-particle biped. The instantaneous center of rotation alternates between the southern and the northern foot. In Fig. 2d we plot the simulated and experimentally determined total, longitudinal and transversal displacement of the instantaneous center of rotation as a function of the length b of the biped. The displacement is shown for a loop of width $\Delta\phi = 70^\circ$ for the simulations and $\Delta\phi = 65^\circ$ and $\Delta\phi = 200^\circ$ for the experiments. The total simulated displacement induced by the control loop is a primitive unit vector for small bipeds and increases by two lattice constants when the biped length times the sine of half the azimuthal loop width $b_t \sin(\Delta\phi/2) = na$ is an integer multiple of the length of the unit vector. The experimental displacement shows similar behavior, however also even displacements are observed when $b_t \sin(\Delta\phi/2)/a$ is close to an integer. Presumably this occurs because the control loop is not entirely symmetric around Q_2 such that the two higher order fences pass through the loop at slightly different biped sizes. Comparing the simulated and experimental total displacement we find excellent agreement.

We also depict the longitudinal and transversal displacement of the instantaneous center of rotation. The longitudinal displacement $\Delta r_l = a_1 b \sin(\Delta\phi/2)/a$ is proportional to the biped length b and increases continuously with the length of the biped. The transversal displacement does not exceed the length of a primitive unit vector $\Delta r_t = 2a_1(b \sin(\Delta\phi/2)/a - \text{round}[b \sin(\Delta\phi/2)/a])$. If we decompose the experimental displacement into longitudinal and transversal displacement we find the experimental longitudinal component to be systematically lower than the longitudinal component of the simulations. The experimental transversal component shows some trend to follow the discontinuous behavior of the transversal simulated component. We believe this relatively poor agreement to arise from the fact that in contrast to the total displacement the individual displacements are not topologically protected, but are susceptible to weak perturbations such as imperfections of the lithographic pattern, misalignments between the control loop and the pattern, and the deviation of the colloidal biped from an idealized paramagnetic line.

6.2 Center gauge

For a better understanding of the topology of the motion the center gauge is more useful and the potential in this gauge reads (see eqn (3)):

$$V_{\text{biped}} \propto (\psi(\mathbf{r} + \mathbf{b}/2)) - (\psi(\mathbf{r} - \mathbf{b}/2)) \quad (10)$$

with the biped centered at the position \mathbf{r} . The biped potential is periodic and invariant under the simultaneous transformation $\mathbf{b} \rightarrow \mathbf{b} + \mathbf{a}$ and $\mathbf{r} \rightarrow \mathbf{r} + \mathbf{a}/2$ where \mathbf{a} is a primitive lattice vector. The biped potential reverses sign $V_{\text{biped}} \rightarrow -V_{\text{biped}}$ when one reverses the biped vector $\mathbf{b} \rightarrow -\mathbf{b}$. The fence is the set

$\mathcal{F} = \{(\mathbf{r}_A, \mathbf{b}) | \nabla_A V_{\text{biped}} = 0 \text{ and } \det(\nabla_A \nabla_A V_{\text{biped}}) = 0\}$. Its projection into \mathcal{C} is the set $\mathcal{F}_{\mathcal{C}} = \{\mathbf{b} | (\mathbf{r}_A, \mathbf{b}) \in \mathcal{F} \text{ for some } \mathbf{r}_A\}$.

In Fig. 2a we construct the projection of the fence onto the spherical control space of a biped of finite length b on a square pattern from that of a colloidal sphere (a point particle see ref. 24). For convenience we show the control space of a biped of length b as a sphere of radius b . Pieces of three such spheres are shown in Fig. 2a. As for point particles zero order fences lie along the b_1 and b_2 coordinates. Because the biped potential is periodic in \mathbf{b} with period \mathbf{a} these zero order fences repeat as higher order fences every lattice vector (gray and black lines in Fig. 2a). The minima near the black fences are displaced from the minima near the gray fences by half the lattice vector. For small bipeds $b < a$ the control space is topologically equivalent to that of a point particle. Larger biped control spaces are cut also by higher order fences displaced from the origin and are therefore topologically different from small biped control spaces with more fence points on the equator. Each winding of a control loop around one of the fences adiabatically propels the biped by a unit vector perpendicular to the fence. The fundamental loop $\mathcal{L}_{-Q_2}^{-1}(\Delta\phi)$ in Fig. 2a winds clockwise around the central fence along the $-b_2$ axes for all biped sizes but also around the black displaced fences parallel to the b_2 -axes for the $b = 2.1a$ bipeds. The $b = 2.1a$ bipeds therefore are propelled three times as fast as the small bipeds. Much alike human beings bipeds with longer legs move faster than smaller bipeds. The increase in speed however happens in discrete steps as the speed is topologically enforced to be a multiple of a lattice vector per cycle.

The walker gauge may shed some light on what part of the motion is true walking and what part is sliding. In contrast to the gauge independent description in terms of winding numbers the decomposition into active and passive motion relies on a gauge and does not survive a gauge transformation.

7 Selective combinations of fundamental loops

The control space of the square lattice in Fig. 2a contains fence points at the positions

$$\phi_{\mathcal{F},n,m} = \arcsin \frac{na}{b} + m \frac{\pi}{2}. \quad (11)$$

with $m = 0, 1, 2, 3, \dots$ and n an integer. For bipeds larger than the lattice constant ($b > a$) fundamental loops around these new $n \neq 0$ fence points will not transport small bipeds, but only bipeds of the proper length. Moreover, the azimuthal position for the higher order fences depend on the biped length $\left(\frac{d\phi_{\mathcal{F}}}{db} \neq 0\right)$, allowing to adiabatically transport larger bipeds

that fall into the appropriate length range. In Fig. 3a, we show the complex loops in control space that transport small bipeds into the $-x$ -direction and bipeds consisting of four colloids of biped length $b = (4 - 1)2R$ into the $+x$ -direction. In Fig. 3b the four colloids are transported in the $+y$ -direction perpendicular

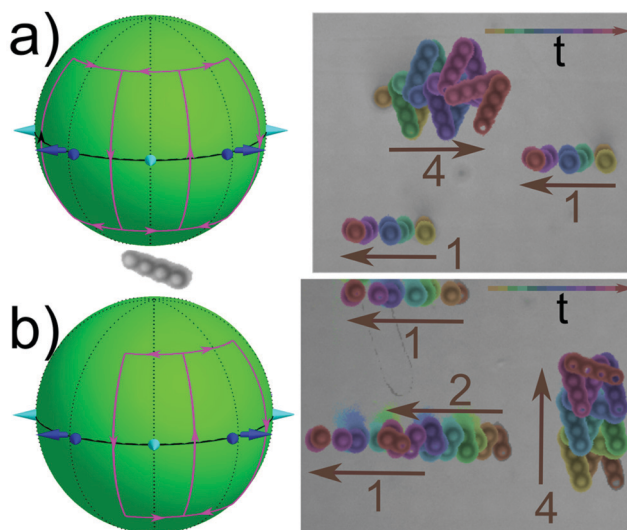


Fig. 3 (a) Control space for a biped consisting of four colloids ($b = (4 - 1)2R$) together with a loop encircling the zero order y -fence in the positive and the 1st order x - and y -fences in the negative sense. Bipeds consisting of four colloids are transported in the $+x$ -direction while single colloidal particles are transported in the $-x$ -direction. We show an overlay of microscope images of the same bipeds at different times with the different times color coded from yellow toward red. (b) The same control space as in (A) subject to a loop encircling the zero order y -fence in the positive and the 1st order x - and y -fence in the negative sense. Bipeds consisting of four colloids are transported in the $+y$ -direction while single colloidal particles and doublets are transported in the $-x$ -direction. An overlay of microscope images of various bipeds is provided using the same color coding as in (A). Videoclips showing the complementary motion of different bipeds subject to the complex loops in this figure are shown in the Supplementary movie adfigure3.mp4.

to the single colloid transport direction. A video clip showing the complementary motion of different bipeds subject to these complex loops are shown in the Supplementary movie adfigure3.mp4. The longer the biped the more fence points exist in control space and the more directions of motion can be invoked by the proper combination of fundamental loops. A protocol how to exploit the fence pattern in a systematic way can be found in ref. 30.

8 Topological effects of hydrodynamic friction

The topological protection of the walker is based on the fact that the grounded foot of the walker remains within its local foothold as long as we do not approach the equator of control space where the transition of the foothold of the left toward the right foot occurs. For this the instantaneous center of rotation must remain with the grounded foot.

In a low Reynolds number fluid hydrodynamic friction opposes the rotation of a biped with the external field. The hydrodynamic friction of a rotating stick is minimal when the instantaneous center of rotation is centered in the biped rather than in one of its feet. Increasing the speed of the control loop

therefore causes competition for the instantaneous center of rotation between the biped center and the biped feet.

When the hydrodynamic forces exceed the pattern forces, which happens especially when the biped foot to foot vector endpoint is close to one of the fences, one may lose an integer number of steps per loop. The Mason number $\mathcal{M} = \eta 2\pi f / \mu_0 \chi_{\text{eff}} \mathbf{H}_{\text{ext}} \mathbf{H}_p$ (with η the shear viscosity of the fluid and χ_{eff} the effective magnetic susceptibility of a colloidal particle) is a dimensionless measure of the driving frequency $f = T^{-1}$ of a loop. In Fig. 4a, we plot Brownian simulation data of the number of steps of a biped *versus* its effective length $b \sin(\Delta\phi/2)/a$ and *versus* the dimensionless frequency $\mathcal{M}(b/a)^{3/2}$. The topological protection of an integer number of steps of the biped also holds when the driving is not adiabatic. However, the faster the driving the lower the number of biped steps per loop.

The experimental data in Fig. 4b shows odd and even steps and roughly follows the simulations. The lack of detailed

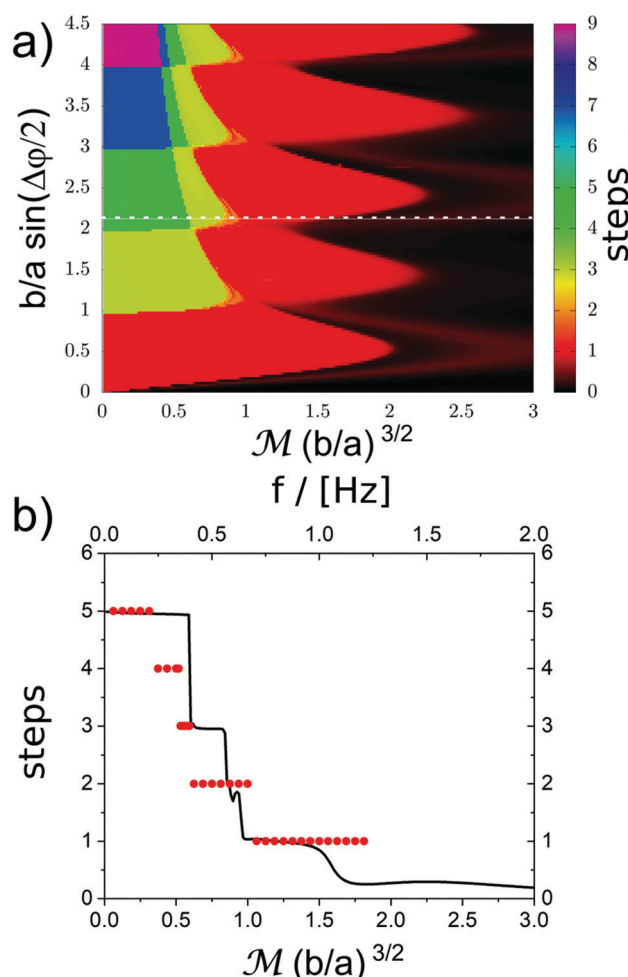


Fig. 4 (a) Brownian dynamics simulations of the displacement of the biped as a function of the Mason number and the effective length of the biped. (b) The experimental data of a biped of length $b/a \sin \Delta\phi/2 \approx 2.1$ versus the frequency of the driving (red circles) and the simulated data for the same effective length versus Mason number.

agreement may be easily understood as we have neglected the presence of the solid support as well as hydrodynamic interactions between the colloidal beads in the simulations. However, the topological locking to integer steps seems to be a robust feature of the dynamics also at higher frequencies.

9 Symmorphic hexagonal pattern

9.1 Control space

In Fig. 5a we plot the fence (red and blue) in the Wigner Seitz cell (cyan) of a hexagonal lattice as a function of \mathbf{b} . In theory we could in principle also change the length of the biped such that our control space is augmented by one dimension. In the experiments the biped length will be fixed and the control space is the cut of a sphere of radius b with this augmented control space. In Fig. 5a fence areas are bordered by bifurcation lines (yellow, magenta, and cyan) with the bifurcation lines meeting in topological transition points that are located in the center and at the corners of the Wigner Seitz cell. A cut of the periodically continued fence with a sphere of radius b constitutes the control space \mathcal{C} of a biped of fixed length b . In Fig. 5b we show the normalized spherical control spaces for $(b = 0.33a, b_t = a/\sqrt{3}, 0.7a)$ and $b_t = a$. If the fence segments of two bipeds can be continuously deformed into each other without changing the number of bifurcation points the bipeds exhibit equivalent transport behavior. The behavior of the bipeds changes at the topological transition lengths $b_t = a\sqrt{(n^2 + nm + m^2)/3}$, where n and m are integers.

If we project the bifurcation lines of Fig. 5a to the plane $b_z = 0$ we obtain the projected fence lines in Fig. 5c. The yellow line segments between the topological transition points are along the lattice vectors and the magenta (cyan) segments are parallel to the positive (negative) reciprocal lattice vectors when folded into the Wigner Seitz cell. The cyan segments are anti parallel to the positive reciprocal lattice vectors. The circle of biped length b cuts through

theses segments and the number N_a (N_Q) of yellow (magenta or cyan) segments cut exactly once are the number of bifurcation points of type B_a and B_Q in the northern fence in Fig. 5b.

9.2 Stationary manifold

For a fixed length of the biped the stationary manifold $\mathcal{M} = \{(\mathbf{r}_A, \mathbf{b}) | \nabla_A V_{\text{biped}} = 0\} \subset \mathcal{C} \otimes \mathcal{A}$ can be shown to be a manifold of genus $g = N_a + N_Q - 5$ that is cut into three pieces \mathcal{M}_+ and \mathcal{M}_- of genus $g_+ = g_- = (N_a - 2)/2$ and, \mathcal{M}_0 of genus $g_0 = N_Q - 3$, where the stationary points are maxima, minima, respectively saddle points of the biped potential. The holes in $\mathcal{C} \otimes \mathcal{A}$ and in \mathcal{M} are inherited from the holes of \mathcal{A} (a torus). A loop $\mathcal{L}_C \subset \mathcal{C}$ in control space has several preimage loops $\mathcal{L}_{\mathcal{M}_i} \subset \mathcal{M}$, ($i = 1, 2, \dots, m$), ($m = 4, 5$, or 6) on \mathcal{M} . If one of these loops entirely lies in \mathcal{M}_- and winds around holes in \mathcal{M}_- the loop will be projected into action space as a minimum loop $\mathcal{L}_A \subset \mathcal{A}$ that winds around the torus and therefore adiabatically transports the biped. Fundamental loops in control space that enter and exit the region north of the fence *via* fence segments of the same color (red or blue) cause adiabatic transport. A preimage loop that winds around holes of \mathcal{M}_- but crosses over to \mathcal{M}_0 also transports but in form of a ratchet. Fundamental loops in control space that enter and exit the region north of the fence *via* fence segments of different color cause ratchet transport. At fixed biped length b one form of adiabatic transport changes to another form of adiabatic transport only *via* an intervening ratchet. The adiabatic speed of a longer biped can be higher once we insert more bifurcation points of type B_a into a fence in control space and this happens the first time for $b > a$ beyond the lowest fence in Fig. 5b and c.

9.3 Response to loops in action space

The hexagonal pattern lacks a glide plane and the fence is no longer located at the equator but in the northern hemisphere, and the number of minima of the potential per unit cell of the

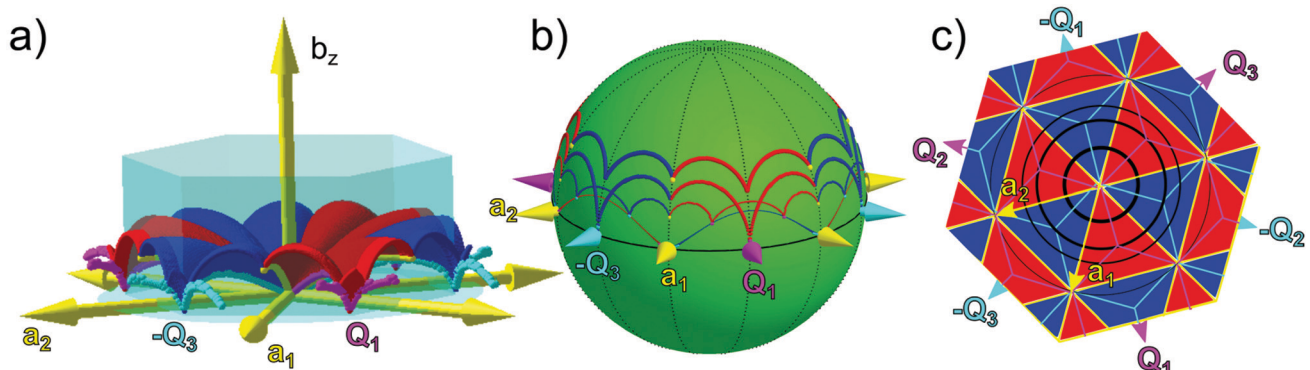


Fig. 5 (a) Fences (red and blue) within the Wigner Seitz cell (cyan) of a hexagonal lattice with unit vectors \mathbf{a}_1 and \mathbf{a}_2 . Bifurcation lines (yellow, cyan and magenta) are lines where the curvature of the fences diverges. The bifurcation lines meet at topological transition points located in the center and at the corners of the Wigner Seitz cell. (b) Fence segments and bifurcation points on the control space \mathcal{C} of the external field obtained from figure (a) by cutting the fence with a sphere of radius $b = 0.33a$ (upper fence), $b_t = a/\sqrt{3}$, $b = 0.7a$, and $b_t = a$ (thinnest fence) and projecting it to a unit sphere. Topologically nontrivial loops must wind around one of the bifurcation points of the biped. There are modulation loops that circle around a bifurcation point of a biped of one but not the other length. (c) Projection of the bifurcation lines of figure (a) in an extended zone scheme onto the plane $b_z = 0$ together with cuts (black) of the spheres from (b) with this plane. Topological transitions in the biped behavior occur when ever the radius moves across one of the topological transition points.

lattice differs depending on whether the external field is north or south of the fence. For this reason, even if we apply a loop that extends as much to the north as to the south of control space, the motion of the biped is a limping motion. We see this in Fig. 6 by the instantaneous center of rotation (green) meeting the southern (blue) foot within a southern foothold (bubble) and the northern (red) foot within one of the two (white) interstitials between three bubbles. When the motion is adiabatic the northern foothold can hold the northern foot at its location while we exit the region of control space north of the fence. In contrast, for a ratchet the northern foot of the biped prior to crossing the fence is in a vanishing foothold and therefore irreversibly jumps to the remaining foothold in the other interstitial when we exit the northern region. Simultaneously the southern foot jumps above the southern foothold (bubble). During the jump the orientation of the biped is fixed and therefore the instantaneous center of rotation moves away from the northern foothold far above the magnetic pattern before it returns to the northern foot after the jump. The northern foot stays with the remaining northern foothold only for the short period of the loop from the fence to the equator. The southern foot touches down to the southern foothold when we cross the equator, and the adiabatic propulsion caused by the northern segment of the loop in control space is booked in the walker gauge by a transfer of the instantaneous center of rotation from the northern to the southern foot. In Fig. 6a we show the control space of a biped of length $b = 1.4a$ with 36 red and blue fence segments north of the equator. A symmetric loop around $-Q_3$ enters and exits the north of control

space via a red fence segment and thus causes an adiabatic walk simulated with Brownian dynamics to the right of Fig. 6b. A different asymmetric loop in Fig. 6a enters the north of \mathcal{C} via a blue segment and exits via the same red fence segment as the symmetric loop. Upon entry the northern foot resides in a foothold that vanishes upon exit through the red fence and therefore jumps to the remaining foothold, *i.e.* the remaining foothold in which the southern foot of the adiabatic loop had stayed in through the entire northern part of the adiabatic loop. The net motion is $-2a_3$ for the symmetric loop and $-a_2 - a_3$ for the asymmetric loop.

In Fig. 6c we show the experimental trajectories of two bipeds of length $b = 1.2a$ subject to an asymmetric and a symmetric loop, the first performing a ratchet motion, the second an adiabatic motion. Ratchet jumps are visible as a motion of higher speed, with both feet making parallel displacements such that the relative orientation of the feet remain the same. Note that the adiabatic trajectories are mirror symmetric such that it is not possible to tell the direction of the motion from the trajectories. The ratchet trajectories in contrast are chiral and the direction of the motion can be told from this chirality. The direction is with the southern foot jumping into the bubble not out of the bubble. Similarly, the direction can be inferred from the northern foot jumping from the foothold that is the center of curvature of the arc segment of the southern foot toward the foothold that is not a center of curvature of an arc segment of the southern foot. In the video clip adfigure6.mp4 the motion of the two experimental bipeds can be followed in full detail. The computation of the

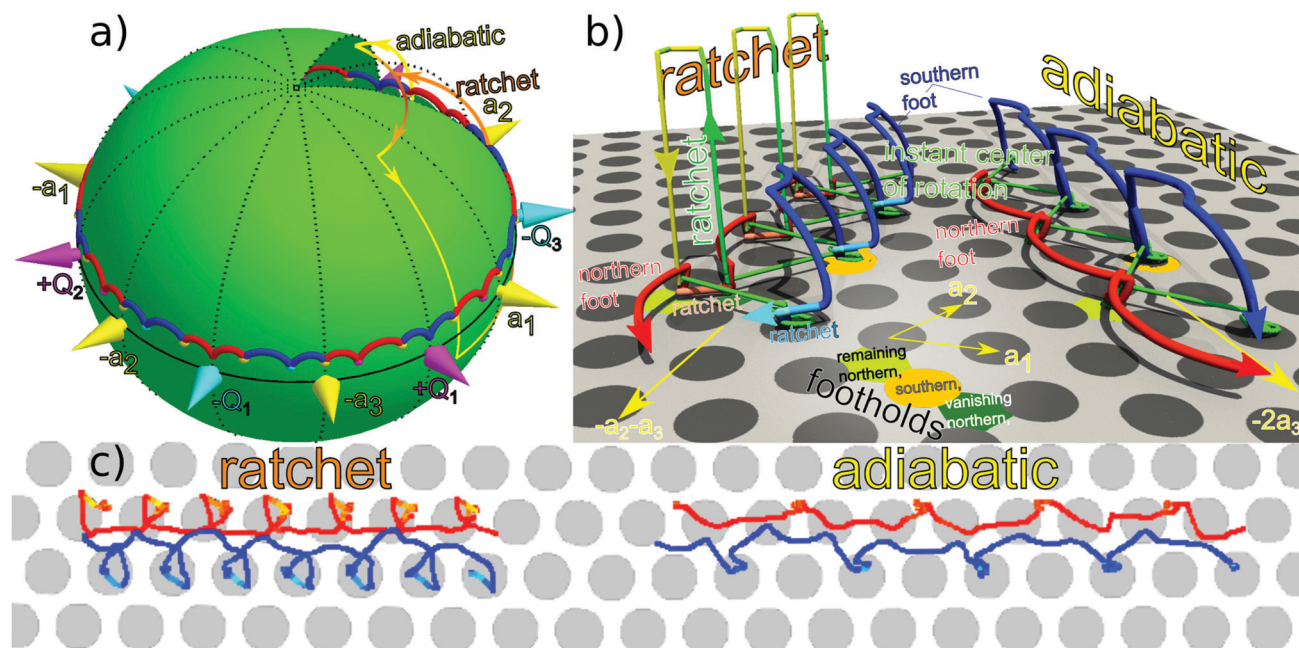


Fig. 6 (a) Control space and fence of a biped of length $b = 1.4a$ with an asymmetric control loop causing a ratchet and a symmetric control loop causing adiabatic transport. (b) Simulated trajectories of the northern and southern foot and the instantaneous center of rotation of the same biped for the asymmetric and for the symmetric loop. In the ratchet trajectories brighter colors of the trajectories label the regions of higher speed when the ratchet jumps occur. (c) Experimentally measured ratchet and adiabatic trajectories of the feet of the bipeds of lengths $b = 1.2a$ and $b = 1.4a$ respectively. The trajectories are colored with brighter colors where the velocity is higher. Videoclips of the two experimental bipeds are shown in the Supplementary movie adfigure6.mp4.

instantaneous center of rotation from the motion of the two feet is rather sensitive to noise in the measurements and led to results dominated by the noise for these experiments. We do not show the instantaneous centers of rotation of the two experiments for this reason.

10 Discussion

The bipeds studied in this work are rigid bipeds having no joints. For these bipeds it is straight forward to compute the winding numbers of the driving loops in control space. Some of the objects one winds around are fixed and do not move with the size of the biped. Higher order objects arising from the periodicity of the problem as a function of the biped vector \mathbf{b} move in control space as the length of the biped grows. Part of the motion is therefore topologically protected independently of the size, others only beyond a certain size and only if one adapts the modulation loop to the increasing size.

Robotic bipeds have joints and other internal degrees of freedom of the conformation of a biped. Which of our findings of this work remain true when dealing with colloidal bipeds that have joints? The answer of course is that everything remains topologically protected if the conformation of a biped with joints does not deviate too strong from that of a rigid rod. In Fig. 7 and in the Supplementary movie adfigure7.mp4 we show the motion of a colloidal biped on a square lattice that is deformed by viscous and magnetic stress³¹ by a loop enclosing the vicinity of the equator. The shape of the biped at large Mason number alternates between an S-shaped conformation (stage 6 in Fig. 7) and its chiral mirror image (stage 4 in Fig. 7).

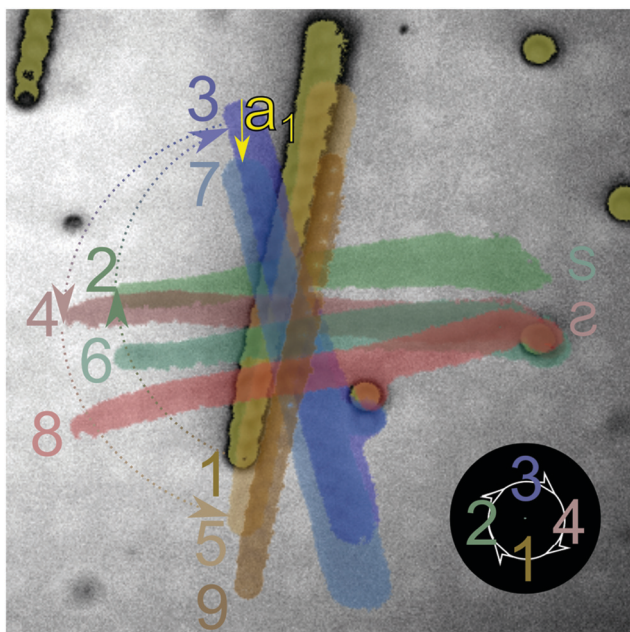


Fig. 7 Overlay of nine microscope images of a shape changing flexible colloidal rod at different times of the driving loop. The shape changing rod performs a topologically protected non-adiabatic walk on the pattern. A videoclip of the biped is shown in the Supplementary movie adfigure7.mp4.

The same biped returns to a straight rod shape as the external field direction moves along the longitudinal sections of the loop. The non-adiabatic walking motion of these bipeds remains locked to a unit vector of the lattice, which proves that also flexible bipeds are topologically protected.

Once the flexibility of a biped becomes substantial we expect them to morph into magnetic filaments the propulsion of which has been studied in great detail.^{32–38} The propulsion of magnetic filaments and bipeds are similar as they both are examples of geometric motion, *i.e.* a motion, where the global displacement only depends on the conformational path of the filaments or bipeds and not on the speed with which the conformational path is taken. Apart from these similarities the process of motion of filaments starkly differs from the motion of bipeds. For a filament to swim one must attach it to a larger particle that breaks the mirror symmetry between the two ends. A mirror symmetric filament would not be able to swim in a bulk low-Reynolds number liquid. Our bipeds are mirror symmetric and they can only walk by interacting with the magnetic pattern to which they intermittently bind but then detach. In the case of filaments the propulsion is a geometric propulsion which is not topological. If one perturbs the driving magnetic field the motion of the filament deviates from the original path, while in our topological system a small perturbation of the driving magnetic field perturbs the path of the motion but not the total displacement after completion of the closed but perturbed modulation loop.

It is not important whether the particles are paramagnetic or ferromagnetic since only the direction of the external magnetic field not its magnitude enters into the topology of the biped potential. We have not tried ferromagnetic colloids, but we anticipate them to behave in the same way, if we could keep them in a biped-shape and prevent the formation of closed rings.

A decrease of the scale will render thermal fluctuations more important and will broaden the bifurcation points into local regions that must be avoided in control space for the transport to remain robust. The robust biped motion control might be relevant for lab-on-the-chip applications.

11 Conclusions

The adiabatic walking step width of self assembled paramagnetic colloidal rods on a periodic magnetic lattice is topologically locked to be commensurate with the magnetic lattice. For this reason driving loops can be classified by winding numbers around fences (bifurcation points with fence segments) in control space. The walking is robust against a variety of static, adiabatic, and dynamic perturbations of the system. While the description of the absolute motion of the biped is gauge invariant, the decomposition into an active and a passive motion is gauge dependent.

Author contributions

MMK, AdE, DdlH, & TMF designed and performed the experiment, and wrote the manuscript with input from all the other

authors. MU & FS produced the magnetic film. AT, RH, IK, ArE & DH performed the fabrication of the micromagnetic domain patterns within the magnetic thin film.

Conflicts of interest

There are no conflicts to declare.

Appendix

We use Brownian dynamics to simulate the motion of the bipeds on top of the magnetic pattern. Each biped consists of N particles where each particle sees the magnetic potential

$$V(\mathbf{x}_A, \mathbf{H}_{\text{ext}}(t), z) \propto -\mathbf{H}_{\text{ext}}(t) \cdot \mathbf{H}_p(\mathbf{x}_A) e^{-(z-z_0)^{\frac{2\pi}{a}}}, \quad (12)$$

where $\mathbf{H}_{\text{ext}}(t)$ is the external field at time t , $\mathbf{H}_p(\mathbf{x}_A)$ is the magnetic field created by the pattern at a fixed height z_0 above the pattern at the position of the particle position \mathbf{x}_A in action space \mathcal{A} and z is the distance of the particle from the pattern. The equation of motion is then given by

$$\xi \dot{\mathbf{x}}_A(t) = -\nabla_{\mathcal{A}} V(x_A, \mathbf{H}_{\text{ext}}(t), z) + \eta(t), \quad (13)$$

where ξ is the friction coefficient and η is a Gaussian random force with a variance given by the fluctuation-dissipation theorem. We use a constant value of ξ which neglects all hydrodynamic interactions between the particles. The equation is then integrated in time t with a standard Euler algorithm. To restore the rigid shape of the biped and the enslavement of the orientation \mathbf{b} to the external magnetic field $\mathbf{H}_{\text{ext}}(t)$, after every simulation step the center \mathbf{x}_c of the biped is determined by the mean position of all particles

$$\mathbf{x}_c(t) = \frac{1}{N} \sum_{i=1}^N \mathbf{x}_i(t) \quad (14)$$

and its direction \mathbf{b} by the direction of the external field \mathbf{H}_{ext} . The new position for every particle is calculated as

$$\mathbf{x}_i(t) = \mathbf{x}_c(t) + (2i - (N+1)) \frac{\mathbf{R}}{\mathbf{H}_{\text{ext}}(t)} \cdot \mathbf{H}_{\text{ext}}(t), \quad (15)$$

$$i = 1, \dots, N.$$

The particles are then shifted the same amount along an axis perpendicular to the pattern such that the lowest particle has the distance z_0 from the pattern. We use a time step dt in the range from $\frac{T}{dt} \approx 2 \times 10^4$ to 2×10^5 , where the period T is proportional to the arc length S of the modulation loop in control space \mathcal{C} .

Acknowledgements

This work is funded by the Deutsche Forschungsgemeinschaft (DFG, German Research Foundation) under project number 440764520. M. U. and F. S. acknowledge support from the Polish National Agency for Academic Exchange under grant number PPN/BDE/2019/1/00014/U/00001.

References

- D. Jongenee, R. Withagen, R. Withagen and F. T. J. M. Zaal, Do children create standardized playgrounds? A study on the gap-crossing affordances of jumping stones, *J. Environ. Psychol.*, 2016, **44**, 45–52.
- A. Yildiz, M. Tomishige, R. D. Vale and P. R. Selvin, Kinesin walks hand-over-hand, *Science*, 2004, **303**, 676–678.
- C. L. Asbury, Kinesin: world's tiniest biped, *Curr. Opin. Cell Biol.*, 2005, **17**, 89–97.
- M. L. Shik and G. N. Orlovsky, Neurophysiology of locomotor automatism, *Physiol. Rev.*, 1976, **56**, 465–501.
- D. Hamacher, F. Herold, P. Wiegel, D. Hamacher and L. Schega, Brain activity during walking: A systematic review, *Neurosci. Biobehav. Rev.*, 2015, **57**, 310–327.
- P. Holmes, R. J. Full, D. Koditschek and J. Guckenheimer, The Dynamics of Legged Locomotion: Models, Analyses, and Challenges, *SIAM Rev.*, 2006, **48**, 207–304.
- W. B. Sherman and N. C. Seeman, A Precisely Controlled DNA Biped Walking Device, *Nano Lett.*, 2004, **4**, 1203–1207.
- A. Shapere and F. Wilczek, Geometry of self-propulsion at low Reynolds number, *J. Fluid Mech.*, 1989, **198**, 557–585.
- A. Shapere and F. Wilczek, Efficiency of self-propulsion at low Reynolds number, *J. Fluid Mech.*, 1989, **198**, 587–599.
- Q. Nguyen, H. Ayonga, G. W. Jessy, A. D. Aaron and S. Koushil, 3D Dynamic Walking on Stepping Stones with Control Barrier Functions 2016 IEEE 55TH CONFERENCE ON DECISION AND CONTROL (CDC), IEEE Conference on Decision and Control, 2016, pp. 827–834.
- M. Z. Hasan and C. L. Kane, Colloquium: Topological insulators, *Rev. Mod. Phys.*, 2010, **82**, 3045–3067.
- S.-Q. Shen, *Topological insulators: Dirac equation in condensed matters*, Springer Science, and Business Media, 2013.
- M. C. Rechtsman, J. M. Zeuner, Y. Plotnik, Y. Lumer, D. Podolsky, F. Dreisow, S. Nolte, M. Segev and A. Szameit, Photonic Floquet topological insulators, *Nature*, 2013, **496**, 196–200.
- M. Xiao, G. Ma, Z. Yang, P. Sheng, Z. Q. Zhang and C. T. Chan, Geometric phase and band inversion in periodic acoustic systems, *Nat. Phys.*, 2015, **11**, 240–244.
- A. Murugan and S. Vaikuntanathan, Topologically protected modes in non-equilibrium stochastic systems, *Nat. Commun.*, 2017, **8**, 13881.
- A. M. E. B. Rossi, J. Bugase and Th. M. Fischer, Macroscopic Floquet topological crystalline steel and superconductor pump, *Europhys. Lett.*, 2017, **119**, 40001.
- C. L. Kane and T. C. Lubensky, Topological boundary modes in isotropic lattices, *Nat. Phys.*, 2014, **10**, 39–45.
- J. Paulose, B. G. Chen and V. Vitelli, Topological modes bound to dislocations in mechanical metamaterials, *Nat. Phys.*, 2015, **11**, 153–156.
- L. M. Nash, D. Kleckner, A. Read, V. Vitelli, A. M. Turner and W. T. M. Irvine, Topological mechanics of gyroscopic metamaterials, *Proc. Natl. Acad. Sci. U. S. A.*, 2015, **112**, 14495–14500.
- S. D. Huber, Topological mechanics, *Nat. Phys.*, 2016, **12**, 621–623.

- 21 M. J. Rice and E. J. Mele, Elementary Excitations of a Linearly Conjugated Diatomic Polymer, *Phys. Rev. Lett.*, 1982, **49**, 1455–1459.
- 22 B. I. Halperin, Quantized Hall conductance, current-carrying edge states, and the existence of extended states in a two-dimensional disordered potential, *Phys. Rev. B: Condens. Matter Mater. Phys.*, 1982, **25**, 2185–2190.
- 23 M. S. Rudner, N. H. Lindner, E. Berg and M. Levin, Anomalous Edge States and the Bulk-Edge Correspondence for Periodically Driven Two-Dimensional Systems, *Phys. Rev. X*, 2013, **3**, 031005.
- 24 D. de las Heras, J. Loehr, M. Lönne and Th. M. Fischer, Topologically protected colloidal transport above a square magnetic lattice, *New J. Phys.*, 2016, **18**, 105009.
- 25 J. Loehr, D. de las Heras, M. Lönne, J. Bugase, A. Jarosz, M. Urbaniak, F. Stobiecki, A. Tomita, R. Huhnstock, I. Koch, A. Ehresmann, D. Holzinger and Th. M. Fischer, Lattice symmetries and the topologically protected transport of colloidal particles, *Soft Matter*, 2017, **13**, 5044–5075.
- 26 C. Chappert, H. Bernas, J. Ferré, V. Kottler, J.-P. Jamet, Y. Chen, E. Cambril, T. De-Volder, F. Rousseaux, V. Mathet and H. Launois, Planar patterned magnetic media obtained by ion irradiation, *Science*, 1998, **280**, 1919–1922.
- 27 P. Kuświk, A. Ehresmann, M. Tekielak, B. Szymański, I. Sveklo, P. Mazalski, D. Engel, J. Kisielewski, D. Lengemann, M. Urbaniak, C. Schmidt, A. Maziewski and F. Stobiecki, Colloidal domain lithography for regularly arranged artificial magnetic out-of-plane monodomains in Au/Co/Au layers, *Nanotechnology*, 2011, **22**, 095302.
- 28 J. Loehr, M. Lönne, A. Ernst, D. de las Heras and Th. M. Fischer, Topological protection of multiparticle dissipative transport, *Nat. Commun.*, 2016, **7**, 11745.
- 29 D. Harland and N. S. Manton, Rolling Skyrmions and the nuclear spin-orbit force, *Nucl. Phys. B*, 2018, **935**, 210–241.
- 30 M. Mirzaee-Kakhki, A. Ernst, D. de las Heras, M. Urbaniak, F. Stobiecki, J. Gördes, M. Reginka, A. Ehresmann and Th. M. Fischer, Simultaneous polydirectional transport of colloidal bipeds, *Nat. Commun.*, 2020, **11**, 4670.
- 31 S. Melle and J. E. Martin, Chain model of a magnetorheological suspension in a rotating field, *J. Chem. Phys.*, 2003, **118**, 9875–9881.
- 32 C. Goubault, P. Jop, M. Fermigier, J. Baudry, E. Bertrand and J. Bibette, Flexible Magnetic Filaments as Micromechanical Sensors, *Phys. Rev. Lett.*, 2003, **91**, 260802.
- 33 R. Dreyfus, J. Baudry, M. L. Roper, M. Fermigier, H. A. Stone and J. Bibette, Microscopic artificial swimmers, *Nature*, 2005, **437**, 862–865.
- 34 M. Roper, R. Dreyfus, J. Baudry, M. Fermigier, J. Bibette and H. A. Stone, On the dynamics of magnetically driven elastic filaments, *J. Fluid Mech.*, 2006, **554**, 167–190.
- 35 K. Ērglis, R. Livanovičs and A. Cēbers, Three dimensional dynamics of ferromagnetic swimmer, *J. Magn. Magn. Mater.*, 2011, **323**, 1278–1282.
- 36 A. Cēbers and K. Ērglis, Flexible Magnetic Filaments and their Application, *Adv. Funct. Mater.*, 2016, **26**, 3783–3795.
- 37 J. Wei, F. Song and J. Dobnikar, Assembly of Superparamagnetic Filaments in External Field, *Langmuir*, 2016, **32**, 9321–9328.
- 38 A. Zaben, G. Kitenebergs and A. Cēbers, 3D motion of flexible ferromagnetic filaments under a rotating magnetic field, *Soft Matter*, 2020, **16**, 4477–4483.